energies

MDPI

Article

Quantification of Dyes Generating Photocurrent and/or Photoluminescence in Dye-Sensitized Solar Cells Using Laser Scanning Microscopy

Masaaki Mitsui *, Kyosuke Mori and Reina Kobayashi

Department of Chemistry, College of Science, Rikkyo University, 3-34-1, Nishiikebukuro, Toshima-ku, Tokyo 171-8501, Japan; 15lb017z@rikkyo.ac.jp (K.M.); 13cc097k@rikkyo.ac.jp (R.K.)

* Correspondence: mitsui@rikkyo.ac.jp; Tel.: +81-3-3985-2364

Received: 12 March 2020; Accepted: 8 April 2020; Published: 11 April 2020

Abstract: Photoconversion processes such as electron injection (photooxidation) and dye regeneration (reduction) in dye-sensitized solar cells (DSSCs) occur at considerably inhomogeneous semiconductor/dye/electrolyte interfaces, implying a very high heterogeneity of interfacial photoconversion kinetics. Herein, we present a temporally and spatially resolved investigation of DSSCs comprising a cover glass photoanode with a 100-nm thick TiO_2 layer loaded with the metal-free organic dye sensitizer MK-2, which is performed by employing laser scanning microscopy (LSM) for the simultaneous measurement of the photocurrent (PC) and photoluminescence (PL) of DSSCs under short-circuit conditions. Analysis of PL decay curves and the excitation rate dependences of PC and PL obtained for local (or submicrometric) areas of the MK-2-DSSC allows disclosing and quantifying three types of dyes coexisting in the DSSCs: (i) a dye that only generates PC ("PC-dye," 75% of total dye molecules in the DSSC), (ii) a dye that generates both PC and PL ("PCPL-dye," 20%), and (iii) a dye that only generates PL ("PL-dye," 5%). Considering recent theoretical reports on cyanoacrylic dyes, we propose that the PC-dye and the PCPL-dye are covalently bound on a TiO_2 surface with different adsorption modes (presumably bidentate and tridentate bridging configurations), whereas the PL-dye is noncovalently trapped within a mesoporous TiO_2 film.

Keywords: dye-sensitized solar cells; photocurrent; photoluminescence; microscopy

1. Introduction

Dye-sensitized solar cells (DSSCs) have attracted a great deal of attention owing to their inexpensive production and efficient energy conversion [1–4]. The main components of DSSCs are an adsorbed dye sensitizer (referred herein as S), a mesoporous TiO_2 film deposited on a transparent electrode, and a redox electrolyte (most commonly I^-/I_3^-). Photoelectric conversion in DSSCs proceeds by electron injection from photoexcited dyes (S*) to the conduction band of TiO_2. Subsequently, the oxidized dyes (S^+) thus formed are reduced by redox couples in the electrolyte, which is called dye regeneration. These pivotal processes occur at considerably inhomogeneous TiO_2/dye/electrolyte interfaces in which there are a variety of adsorption densities and binding states of the sensitizer dyes, resulting in nonuniform photoconversion kinetics in the DSSCs.

Of note, photoluminescence (PL) emission from sensitizer dyes has been frequently observed for dye-loaded TiO_2 films [5,6] as well as for DSSC devices [7–9]. In early studies, the decay of such residual PL was interpreted to reflect the electron injection rate (k_{inj}) of the adsorbed dyes. However, ultrafast spectroscopic experiments show that the majority of the electron injection processes occur within subpicosecond time scale, i.e., $k_{inj} \geq 10^{12}$ s^{-1} [10–14], exhibiting much larger constants than the radiative rate constants (k_r) of ruthenium complexes and metal-free organic dyes (typically

k_r = 10^6–10^9 s^{-1}). Currently, it is accepted that the electron injection rate spans at least six orders of magnitude (10^7–10^{13} s^{-1}). Hence, the residual PL originates from dye molecules that either inject electrons at an exceptionally slow rate or do not undergo electron injection at all, being its origin still elusive. From this viewpoint, Hofkens and coworkers investigated the residual PL behavior of a Ru-type dye on mesoporous films and nanoparticles of TiO_2 using femtosecond transient absorption and time-resolved PL spectroscopic techniques [5]. They concluded that the residual PL is likely to originate from dye molecules noncovalently bound to surface defects, and the covalently bound dye that contributes to the observed PL is negligible, constituting less than 0.1% of the covalently bound dye. The PL decay rate constants of Ru complexes (without electron injection process) are relatively small (typically 10^6–10^7 s^{-1}), which enables to maintain relatively high electron injection yields even at very slow injection rates of, for example, k_{inj} ~ 10^8 s^{-1}. Although Ru complexes have been intensively studied, metal-free organic dye sensitizers have also been attracting great research attention, and have been often utilized in DSSCs [2]. As a benefit, the latter have much larger molar absorption coefficients than Ru complexes; however, this property is inevitably accompanied by one or two order(s) of magnitude larger radiative rate constants (k_r = 10^8–10^9 s^{-1}) than those of Ru complexes. For organic dye systems, it is thus anticipated that covalently bound dye molecules could contribute to not only photocurrent (PC) generation but also PL generation. In this case, either PL or PC measurements alone are insufficient, or a combination of both is essential for the quantification of dyes contributing to PC and/or PL.

Laser scanning microscopy (LSM) probing PC is a spatially resolved characterization technique that has been used for the investigation of DSSCs [15–19]. As shown in Figure 1a, we fabricated a DSSC comprising a cover glass photoanode with a 100-nm thick TiO_2 layer, which allows analyzing the DSSC devices using an oil-immersion objective lens with a high numerical aperture (N.A. > 1), as schematically depicted in Figure 1b [20]. This setup provides a spatial resolution of ca. 200 nm, which is by a factor of 10 times better than that described in previous reports [15–19]. Using this setup, we evaluated photovoltaic parameters such as short-circuit current density (J_{sc}) and open-circuit voltage (V_{oc}) for a local area of the DSSCs. Additionally, analysis of the PC saturation behavior based on a three-state kinetic model quantitatively provides the dye adsorption number (N_c) and dye regeneration rate constant (k_{reg}) at a submicrometric area of the DSSCs [20]. In this contribution, our newly developed LSM for determining PC and PL is applied for DSSCs using a metal-free organic dye sensitizer, MK-2 (Figure 1c), which is an alkyl-functionalized-carbazole dye that exhibits a photoelectric conversion efficiency of 6–8% [21–23]. As a result, three different types of dyes coexisting in the DSSC are quantified: (i) a dye that only generates PC, (ii) a dye that generates both PC and PL, and (iii) a dye that only generates PL.

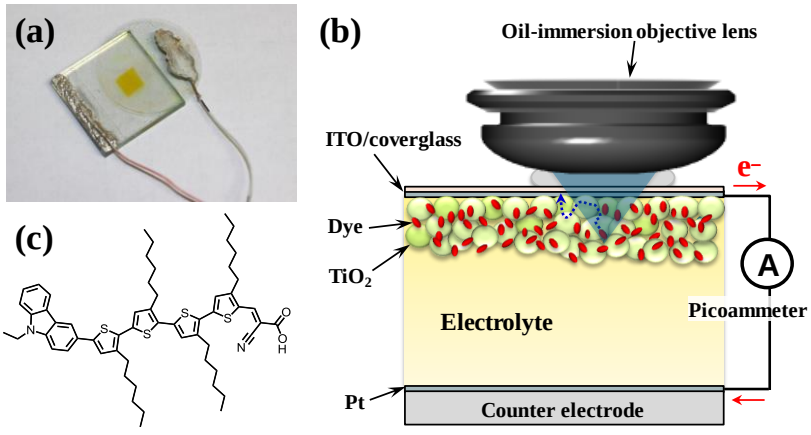

Figure 1. (**a**) Photograph of a dye-sensitized solar cell (DSSC) device with a cover glass photoanode fabricated for laser scanning microscopy (LSM) measurements. (**b**) Schematic of submicrometric LSM setup equipped with an oil-immersion objective lens. (**c**) Molecular structure of the MK-2 dye.

2. Materials and Methods

2.1. Chemicals and Reagents

As the dye sensitizer, MK-2 (2-cyano-3-[5′′′-(9-ethyl-9*H*-carbazol-3-yl)-3′,3″,3′′′,4-tetra-*n*-hexyl-[2,2′,5′,2′′5,′′2′′′]-quarterthiophen-5-yl]acrylic acid), purchased from Sigma-Aldrich, was used without further purification. Toluene, ethanol, 3-methoxypropionitrile, and other reagents were of JIS (Japanese Industrial Standards) special grade and used as received.

2.2. Preparation of Dye-Adsorbed Aluminum Oxide Films

An aluminum oxide (Al_2O_3) semiconductor film was used to estimate the PL lifetime of adsorbed MK-2 with no electron injection process. Ten mg of Al_2O_3 nanopowder (<50 nm particle size and >40 m^2/g BET surface area, Sigma-Aldrich, St. Louis, MO, USA) was dispersed in a mixture of 1 mL ethanol and 1 mL α-terpineol (Special grade, Wako, Osaka, Japan). To form the Al_2O_3 film, one drop of this Al_2O_3 paste was spin-coated onto a thoroughly cleaned cover glass (ϕ22 No.1, Matsunami, Osaka, Japan) and sintered at 250 °C for 30 min. The Al_2O_3-coated cover glass was soaked in 0.1 mM MK-2 dye/toluene solution overnight to adsorb the dye molecules on Al_2O_3. Then, the sensitized film was repeatedly rinsed and sonicated in acetonitrile to remove the physisorbed dye molecules as much as possible. PL lifetime measurements of the MK-2-loaded Al_2O_3 film were conducted under high vacuum conditions (~0.1 Pa) using the LSM setup (mentioned later).

2.3. Cell Fabrication

DSSCs for LSM measurements were prepared as follows. Titanium dioxide (TiO_2) thin films were prepared by spin coating (3000 rpm for 60 s) one drop of Ti-Nanoxide HT-L/SC paste (Solaronix, Aubonne, Switzerland), which contained approximately 3 wt% of 8–10 nm TiO_2 anatase particles, onto thoroughly cleaned indium tin oxide (ITO)-coated cover glasses, 10 Ω/□ (Matsunami), followed by sintering at 250 °C for 30 min. This TiO_2 paste was used to produce a highly transparent scaffolding film approximately 100 nm thick (roughly 2×10^{13} nanoparticles/cm^2), as measured by atomic force microscopy (SPM-9700, Shimadzu, Kyoto, Japan), thereby suppressing light scattering effects upon tightly focused light illumination. The obtained TiO_2 films were carefully shaped to 5×5 mm^2, sonicated with ethanol, and rinsed thoroughly with toluene. The films were then soaked in 0.1 mM MK-2 dye/toluene solution and kept at room temperature for approximately 24 h to complete the dye adsorption. Then, the sensitized films were repeatedly rinsed and sonicated in acetonitrile to remove loosely bound dye molecules. A platinized counter electrode was obtained by spreading a Pt-based solution (Platisol T/SP, Solaronix) on a conductive glass sheet (fluorine-doped tin oxide) of 20×20 mm^2, followed by heating at 450 °C for 30 min. To fabricate a complete solar cell, the counter electrode was assembled with a thermal adhesive film (Meltonix 1170-25PF, Solaronix) that served as a spacer and sealing element. A commercial iodide-based redox electrolyte (Iodolyte Z-50, Solaronix) containing the I^-/I_3^- redox couple ($[I^-] = 1$ M, $[I_2] = 50$ mM), an ionic liquid, *N*-alkylbenzimidazole, and guanidinium thiocyanate in 3-methoxypropionitrile solution was used.

2.4. Photovoltaic Measurement

The current–density versus voltage (*J*–*V*) curves were measured on a computer-controlled potentiostat/galvanostat (HA-501, Hokutodenko, Tokyo, Japan) under illumination of simulated AM 1.5G solar light (100 $mWcm^{-2}$) from a solar simulator (San-ei Electric, Osaka, Japan, XES-40S2-CE with a 150-W Xe lamp and an AM 1.5 filter). The incident light intensity was measured by using a pyranometer (ML-01, Eko, New York, NY, USA).

2.5. Laser Scanning Microscopy (LSM) Measurements

Simultaneous PC and PL measurements were performed on a homemade LSM. A detailed description of the laser scanning method and optical setup of our microscope has been published elsewhere [20,24]. The excitation light was provided by a 478 nm pulsed diode laser (PIL048X, Advanced Laser Diode Systems, Berlin, Germany) operating at 50 kHz–40 MHz and a pulse width of approximately 80 ps full-width at half-maximum (FWHM). The linearly polarized light was focused on a DSSC from the TiO_2-electrode side using an oil-immersion objective lens (100×, N.A. = 1.4, Olympus, Tokyo, Japan) to form a diffraction-limited spot size in the electrode plane. The lateral resolution of the PC and PL measurements conducted using our LSM is ca. 200 nm, which is approximately an order of magnitude smaller than that described in previous studies using the light beam induced current technique [15–19]. As shown in Figure 1b, photocurrent measurements of the DSSCs were conducted at short-circuit using a picoammeter (6487, Keithley Instruments, Cleveland, OH, USA). PL photons from the DSSC samples were collected through the same objective and split by a 50:50 unpolarized beam splitter. Half of the PL signal was sent to a polychromator (SpectraPro 2300i) coupled with a liquid-nitrogen-cooled charge-coupled device camera (Spec-10:100B/LN, Roper Scientific, Lakewood Ranch, FL, USA). The other half was filtered using a 75 μm diameter pinhole for rejection of out-of-focus background, and was directed onto an avalanche photodiode detector (APD; SPCM-AQR-14, Perkin-Elmer, Waltham, MA, USA). The signals from the APD were sent to a time-correlated single photon counting (TC-SPC) card (TimeHarp 200, PicoQuant, Berlin, Germany) in time-tagged and time-resolved mode. Data acquisition and PL decay analyses were performed using SymPhoTime v5.2.4 (PicoQuant) software. To determine the PL lifetime, appropriate exponential functions were fitted to the PL decay curves by maximum likelihood estimation.

In the LSM measurements, PC and PL images of the sample were simultaneously recorded by raster scanning of the laser focal spot. Then, an electronic shutter was used to block the excitation laser light. After the laser focus was moved to the position of interest, the shutter was reopened at the start time of data acquisition. The imaging and positioning processes were controlled by homemade LabView programs. The excitation rate dependences of PC and PL were measured by changing the laser intensity stepwise from high intensity to low intensity. At each laser intensity, a PC and PL time trace was recorded for 10–20 s. The photon detection efficiency at the APD in the present LSM setup (η_{det}) was estimated to be ca. 7%. To accurately estimate the PL intensity, i.e., photon count rate, only from the MK-2 dyes in the DSSCs, the excitation power dependence of background photon count was evaluated for a "no-sensitizer cell," which was fabricated without the dye-sensitization process. Using this calibration, the background photon counts at arbitrary excitation rates were estimated and subtracted from the photon counts detected in the LSM measurements of the DSSCs. All measurements were conducted at room temperature.

3. Results and Discussion

3.1. Photovoltaic Parameters of a Dye-Sencitized Solar Cell (DSSC) Fabricated for Laser Scanning Microscopy

Figure 2a shows a current–density versus voltage (*J*–*V*) curve measured by illuminating a 0.2 cm^2 area of the MK-2-DSSC under AM 1.5G irradiation (100 $mWcm^{-2}$) with an aperture mask. From this curve, the values for the short-circuit current density (J_{SC}), open-circuit voltage (V_{OC}), fill factor (*FF*), and photoconversion efficiency (PCE) were obtained (Table 1). The PCE of previous DSSCs using MK-2 was reported to be 6–8% [16–18]. In contrast, the PCE value of the MK-2-DSSC prepared for LSM was extremely small because the TiO_2 layer was much thinner in this cell than in conventional DSSCs, whose film thicknesses are typically 5–10 μm. However, such a thin film significantly shortens the electron diffusion length in TiO_2, and reduces the probability of recombination of injected electrons with oxidized dye molecules and/or oxidized redox species. Consequently, the DSSCs prepared for LSM possess near 100% collection efficiency of injected electrons at the submicrometric laser illumination (i.e., ~10^{-9} cm^2) [20]. To verify this for the present MK-2-DSSC, the corrected current (I_{dark}), which

was obtained by subtracting the dark current from the light current, was plotted against the applied voltage, as shown in Figure 2b. The photocurrent increased with the applied negative voltage, and became nearly constant around −0.05 V. Therefore, the value of electron collection efficiency (η_{cc}) can be estimated by dividing the value of I_{cor} at 0 V by the saturation value of I_{cor} in a region of negative voltage [25]. According to the curve shown in Figure 2b, a value of 0.95 was obtained for η_{cc}. For any local position, the values of η_{cc} were almost unity (η_{cc} = 0.9–1.0); therefore, the contribution of the charge recombination process can be neglected under local illumination conditions.

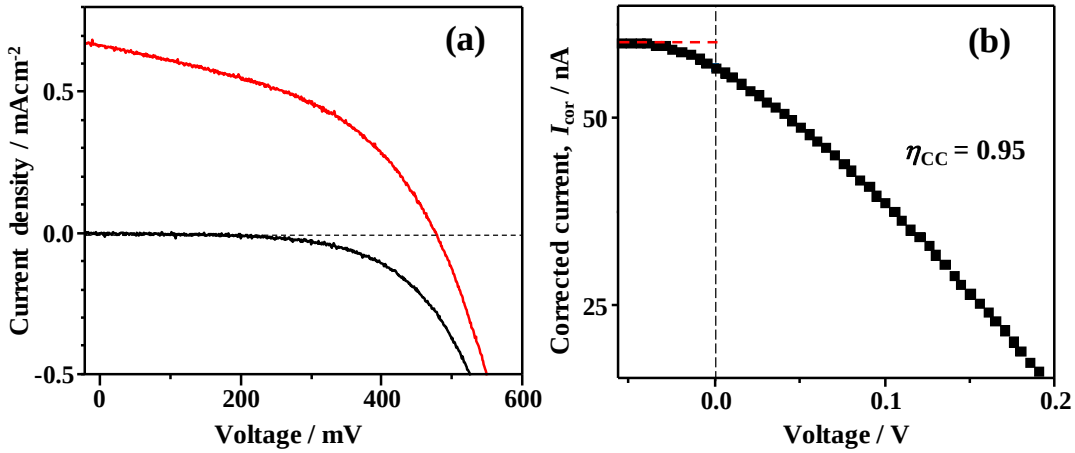

Figure 2. (**a**) Current–density versus voltage (*J*–*V*) curve measured by illuminating a 0.2 cm^2 area of the MK-2-DSSC prepared for LSM under AM 1.5G irradiation (100 $mWcm^{-2}$). (**b**) Corrected photocurrent (I_{cor}) obtained by subtracting dark current from photocurrent measured under short-circuit condition. Note that the plot of I_{cor} was obtained at the submicrometric laser illumination (~10^{-9} cm^2) using LSM. The red dashed line indicates the saturation value of I_{cor}.

Table 1. Photovoltaic parameters, short-circuit current density (J_{SC}), open-circuit voltage (V_{OC}), fill factor (*FF*), and photoconversion efficiency (PCE), of the MK-2-DSSC fabricated for laser scanning microscopy.

Dye	J_{sc}/mAcm^{-2}	V_{oc}/mV	*FF*	PCE (%)
MK-2	0.66	605	0.45	0.14

3.2. Photocurrent and Photoluminescence Images

Figure 3a,b shows PC and PL images simultaneously recorded for the same area in a MK-2-DSSC under short-circuit condition. Owing to the very fast PC response (<1 ms) of the present cells under local (or submicrometric) laser illumination conditions, the PC image can be directly obtained without any corrections of the effect of PC response delay [20]. Several (unintentional) submicrometric structures are observed at the same positions in the PC and PL images. They are likely due to an increased local thickness of the TiO_2 film resulting in increased adsorption or uptake of the MK-2 dye. It is important to note that a strong PL emission is observed for any local area of the DSSC devices. The corresponding PL spectrum shown in Figure 3c exhibits a very broad feature, which contrasts to that of MK-2 in toluene solution. This spectral feature most likely reflects a large inhomogeneity of the surrounding environments of the photoluminescent dyes in the DSSC device.

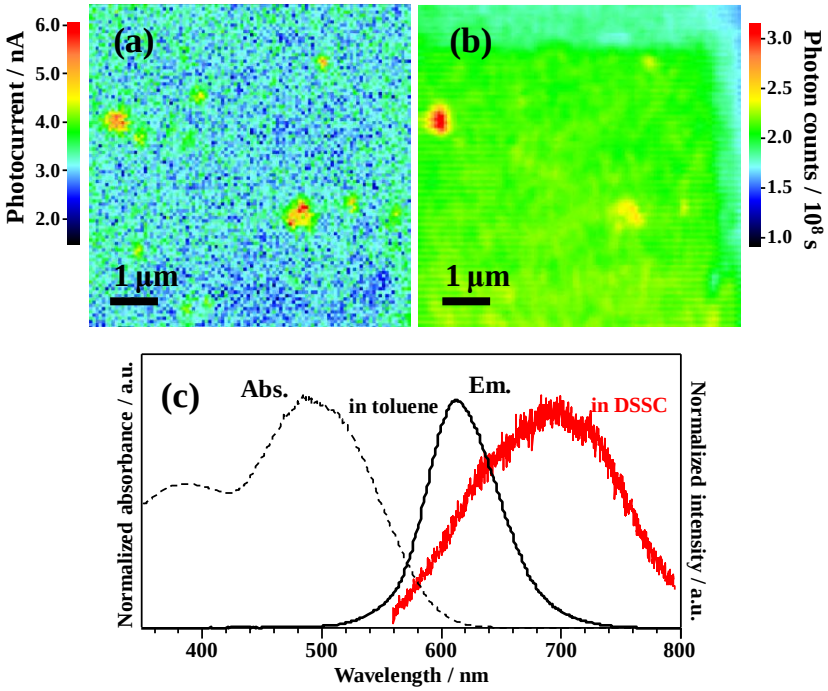

Figure 3. Examples of (**a**) PC and (**b**) PL images simultaneously recorded for the same area in a MK-2-DSSC device. (**c**) Absorption and PL spectra of MK-2 in toluene (black lines) and PL spectrum of MK-2 in the DSSC device (red line).

3.3. Electron Injection

Ultrafast electron injection from MK-2 to the conduction band of TiO_2 (i.e., $k_{inj} > 5 \times 10^{12}$ s^{-1}) has been previously revealed by transient absorption spectroscopy [21]. The radiative rate constant (k_r) of MK-2 in acetonitrile was estimated to be 3.47×10^7 s^{-1} using the relation $k_r = \Phi_{PL}/\tau_{PL}$, which is approximately five orders of magnitude smaller than the electron injection rate. Therefore, the PL of MK-2 on TiO_2 should be completely quenched, i.e., an electron injection yield of 100% should be obtained ($\Phi_{inj} = 1$). As shown in Figure 3b, however, a residual PL emission was also observed for any local area of the DSSC devices, suggesting the coexistence of dyes having low injection yields. To verify this, PL lifetime measurements under local illumination conditions were conducted for 100 different positions of the DSSC. Figure 4a displays the PL decay curve obtained for a local position of the DSSC. It was well-fitted with a double-exponential function described by $I_{PL}(t) = A_1\exp(-t/\tau_1) + A_2\exp(-t/\tau_2)$ with $\tau_1 = 0.46$ ns (the fractional contribution of this component, i.e., $f_1 = A_1\tau_1/(A_1\tau_1 + A_2\tau_2) \times 100$, is 86.2%) and $\tau_2 = 1.16$ ns ($f_2 = 13.8\%$). Similarly, all the PL decay curves could be fitted well with double-exponential functions with the fast and second decay components of approximately 0.5 and 1 ns, respectively. The histograms of f_1 and f_2, which were obtained for 100 local positions in a DSSC, are shown in Figure 4b. The second component is in good agreement with the PL lifetime of MK-2 on Al_2O_3 ($\tau_{PL} = 1.08$ ns), where no electron injection occurs because the conduction band energy of Al_2O_3 (i.e., conduction band edge potential at −4.7 V vs NHE [26]) is much higher than the LUMO energy of the MK-2 dye (−0.89 V vs NHE [21]). Therefore, ca. 18% of photoluminescent MK-2 molecules do not inject photoexcited electrons into TiO_2 at all. We infer that the dye molecules generating only PL (hereafter called "PL-dye") are not covalently bound to the TiO_2 surface, and may form some three-dimensional aggregates on the surface, as was previously reported [21]. On the other hand, the majority of the photoluminescent molecules (82%) are much more efficient for electron injection. These dye molecules generating both PC and PL are hereafter referred to as "PCPL-dye." The electron injection rate constant (k_{inj}) and electron injection yield (Φ_{inj}) at each local position can be obtained using the relations $k_{inj} = 1/\tau_1 - 1/\tau_{Al2O3}$ and $\Phi_{inj} = k_{inj}\tau_1$, respectively. The distributions

of k_{inj} and Φ_{inj} thus obtained are shown in Figure 4c,d, respectively. The average values of k_{inj} and Φ_{inj} obtained by Gaussian fits are summarized in Table 2. Since the mean value of the injection rate, $\langle k_{inj} \rangle$, is 30 times larger than the radiative rate constant ($k_r = 3.47 \times 10^7$ s^{-1}), the value of $\langle \Phi_{inj} \rangle$ is also relatively large ($\langle \Phi_{inj} \rangle = 0.62$).

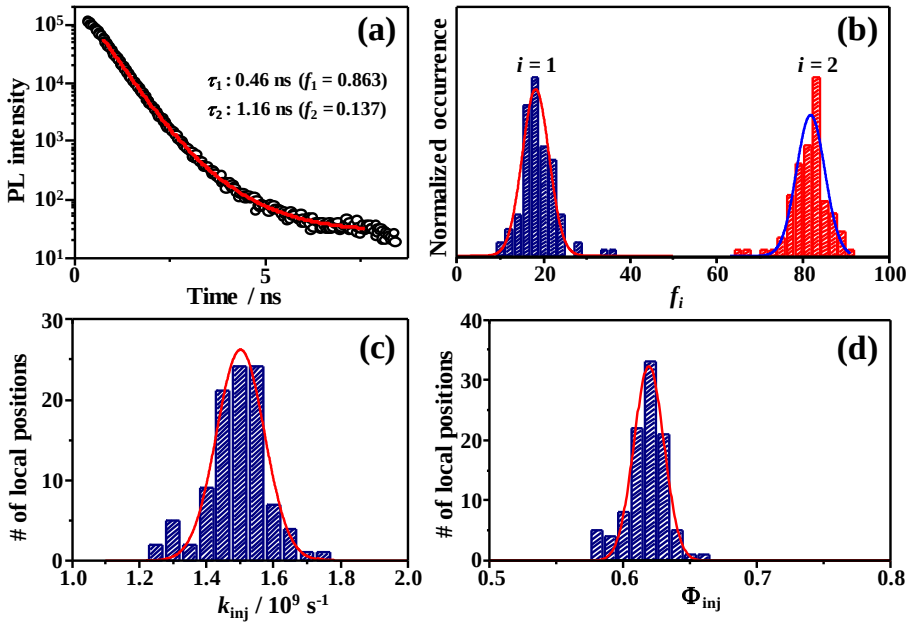

Figure 4. (**a**) PL decay curve of MK-2 in a DSSC recorded under local illumination. The solid line corresponds to a double-exponential fit ($\chi^2 > 0.98$). (**b**) Histograms of the fractional contribution of f_1 and f_2. Histograms of (**c**) electron injection rate (k_{inj}) and (**d**) electron injection yield (Φ_{inj}) obtained for 100 local positions in a MK-2-DSSC device.;

Table 2. Parameters obtained by photocurrent (PC) and photoluminescence (PL) microscopy.

Dye	Type	$\langle N \rangle$ [1]	$\langle k_{inj} \rangle$/s^{-1}	$\langle \Phi_{inj} \rangle$
MK-2	PC-dye	1.14×10^5 (75%)	$>5 \times 10^{12}$	~1
	PCPL-dye	3.09×10^4 (20%)	1.50×10^9	0.62 (0.03) [2]
	PL-dye	6.85×10^3 (5%)	$<10^8$	0

[1] The values in parenthesis are the percentage of each type. [2] The value in parenthesis is the FWHM of the Gaussian fit to the histogram in Figure 4d.

3.4. Excitation Rate Dependence of Photoluminescence Intensity and Photocurrent

3.4.1. Photoluminescence (PL) Analysis

To evaluate the number of "PCPL-dye" molecules per light-exposed volume (N_{PCPL}), we examined the dependence of PL intensity, i.e., photon count rate, on the excitation rate constant (k_{ex}). The total photons emitted from the PCPL-dye per second (P_{PCPL}) is given by:

$$P_{PCPL} = \frac{P_{det}}{\eta_{det}} f_1 \quad (1)$$

where P_{det} represents the detected photons per second at the APD. In Section 3.3, the fractional contribution of the "PCPL-dye" (f_1) has been already evaluated for each local position of the DSSC.

Thus, the values of P_{PCPL} were obtained using Equation (1). On the other hand, the k_{ex} value was calculated by using Equation (2) as follows:

$$k_{ex} = \frac{I_{ex}}{hc/\lambda}\sigma(\lambda) \quad (2)$$

where I_{ex} is the excitation laser intensity in W cm^{-2}, $\sigma(\lambda)$ is the absorption cross section at the excitation wavelength (λ), c is the light velocity, and h is the Planck constant. The value of $\sigma(478) = 1.35 \times 10^{-16}$ cm^2 for MK-2 in toluene was used in the calculation of k_{ex}. As is evident in Figure 5a, the P_{PCPL}–k_{ex} plot obtained for a local position in the DSSC exhibits linear dependence; P_{PCPL} increases linearly with k_{ex}. Similar linear behaviors were observed for any local position of the DSSC. The linear dependence suggests that all the molecules are in the ground state (S_0) when photoexcited. In this case, the excitation rate dependence of P_{PCPL} can be expressed as:

$$P_{PCPL} = \frac{3}{5}k_r\tau_1 N_{PCPL}k_{ex} \quad (3)$$

The coefficient of 3/5 corresponds to the orientational averaging of adsorbed dyes with random orientation against the linearly polarized excitation light [27]. The PL lifetimes (τ_1) of the "PCPL-dye" at each local position were determined in Section 3.3. The k_r value of MK-2 in acetonitrile was estimated to be 3.47×10^7 s^{-1}. Thus, N_{PCPL} is the only unknown parameter in Equation (3), and can be determined by the fit of the P_{PCPL}–k_{ex} plot at the corresponding local position. For example, the P_{PCPL}–k_{ex} plot in Figure 5a is fitted by Equation (3), yielding $N_{PCPL} = 3.09 \times 10^4$ molecules, which corresponds to 0.464 μmol/cm^3 considering the diffraction-limited irradiated volume of 1.36×10^{-9} cm^2 × 100 nm. The number of "PL-dye" molecules (N_{PL}) can also be estimated as $N_{PL} = 4.94 \times 10^3$ molecules using the relation $N_{PL} = N_{PCPL} \times f_2/f_1$. The histograms of N_{PCPL} and N_{PL} are depicted in Figure 5b, and their average values are $\langle N_{PCPL}\rangle = 3.09 \times 10^4$ and $\langle N_{PL}\rangle = 6.85 \times 10^3$ (Table 2). Figure 5c illustrates the correlation plot between N_{PCPL} and N_{PL}, in which a weak negative correlation of −0.46 was obtained; therefore, areas of TiO_2 with lower coverage tend to produce the noncovalently bound PL-dye. These surface areas of TiO_2 may lack a sufficient number of chemisorption sites to allow strong surface binding such as bidentate and tridentate adsorption configurations.

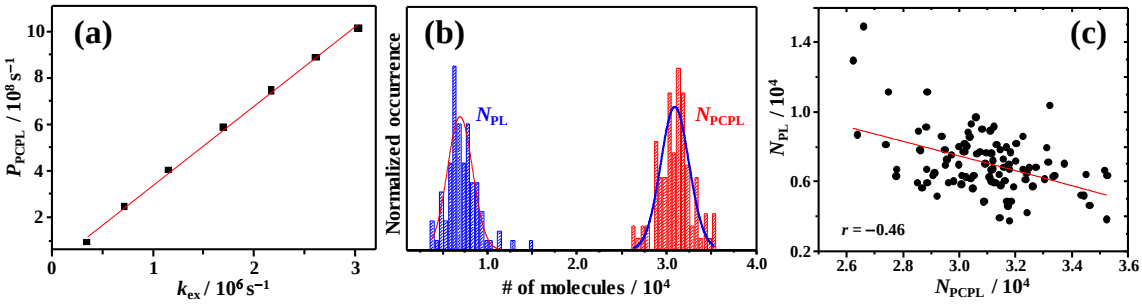

Figure 5. (**a**) Excitation rate dependence of photon count rate of "PCPL-dye" (P_{PCPL}). (**b**) Histograms of the numbers of "PCPL-dye" (N_{PCPL}) and "PL-dye" (N_{PL}) molecules at 100 different local positions of a MK-2-DSSC. (**c**) Correlation plot between N_{PCPL} and N_{PL} (correlation coefficient $r = -0.46$).

3.4.2. Photocurrent (PC) Analysis

As described in Section 3.3, the ultrafast spectroscopic study revealed that some of the adsorbed dyes undergo ultrafast electron injection, with Φ_{inj} values of ca. 1. These dye molecules can be expected to be nonfluorescent and contribute only to PC generation. This type of dye is hereafter referred to

as PC-dye. To evaluate the net PC generated only from PC-dye (I_{PC}), the PC generated from CL-dye (I_{PCPL}) was estimated using Equation (4) as follows:

$$I_{PCPL} = \frac{3}{5} e \Phi_{inj} \eta_{cc} N_{PCPL} k_{ex} \quad (4)$$

where e is the elementary charge. As mentioned above, the values for η_{cc} at any local position are almost unity; therefore, Equation (4) can be approximated to the following Equation (5):

$$I_{PCPL} = \frac{3}{5} e \Phi_{inj} N_{PCPL} k_{ex} \quad (5)$$

Since the values of Φ_{inj} and N_{PCPL} at each local position have already been determined (Figures 4d and 5b), the values of I_{PCPL} can be estimated using Equation (5). The value of I_{PC} can be thus calculated by subtracting I_{PCPL} from the corresponding detected photocurrent (I_{det}), i.e., $I_{PC} = I_{det} - I_{PCPL}$. Figure 6a shows the dependence of I_{PC} on k_{ex}. Similar to the case of PL, the PC also exhibits a linear dependence on k_{ex}. This result contrasts to that obtained for $Ru(bpy)_2(dcbpy)^{2+}$-DSSCs [$Ru(bpy)_2(dcbpy)^{2+}$ = *cis*-bis(2,2′-bipyridine)-(4,4′-dicarboxy-2,2′-bipyridine)ruthenium(II)], where PC saturation was clearly observed with increasing k_{ex} [20]. Such nonlinear behavior can be reasonably explained by the fact that the excitation rate becomes comparable to the decay rate of the oxidized dyes ($k_S{}^+$). Considering that no recombination loss occurs in the MK-2-DSSC (η_{cc} ~1.0), the decay rate of the oxidized dyes corresponds to the dye regeneration rate, i.e., $k_S{}^+ = k_{reg}[I^-]$. The linear behavior of PC suggests that all the oxidized molecules (S^+) return to the ground state until the next photoexcitation; namely, all the molecules are in the ground state (S_0) when photoexcited. Therefore, it is conceivable that the dye regeneration rate ($k_{reg}[I^-]$) of MK-2 is much faster than the excitation rate. Since the concentration of I^- in the electrolyte used in this study is 1.0 M, the magnitude of k_{reg} should be much larger than 10^6 $M^{-1}s^{-1}$. Daeneke et al. reported the driving force (ΔG_{reg}) dependence of k_{reg} for MK-2 using ferrocene derivatives as redox species [28]. According to their results, the regeneration rate constant when using the $I^-/I_3{}^-$ redox couple (ΔG_{reg} = 0.56 eV [21]) was estimated to be approximately 10^8 $M^{-1}s^{-1}$. When [I^-] = 1.0 M, the regeneration rate of MK-2 is almost two orders of magnitude larger than the maximum excitation rate.

The excitation rate dependence of I_{PC} is given by Equation (6):

$$I_{PC} = \frac{3}{5} e \Phi_{inj} \eta_{cc} N_{PC} k_{ex} \quad (6)$$

Both η_{cc} and Φ_{inj} can be approximated to be unity, which allows expressing Equation (6) as follows:

$$I_{PC} = \frac{3}{5} e N_{PC} k_{ex} \quad (7)$$

Thus, N_{PC} can be also determined by the fit of the I_{PC}–k_{ex} plot. The best fit of the plot in Figure 6a was obtained by Equation (7), with N_{PC} = 1.59 × 10^5 molecules (19 μmol/cm^3 on the basis of the volume of local illumination). The histogram of N_{PC} is shown in Figure 6b, and the mean value is $\langle N_{PC} \rangle$ = 1.14 × 10^5 molecules (Table 2). As seen in Figure 6c, there is almost no correlation between N_{PC} and N_{PCPL} (r = −0.26), implying that the "PC-dye" and the "PCPL-dye" are randomly coadsorbed on the TiO_2 film.

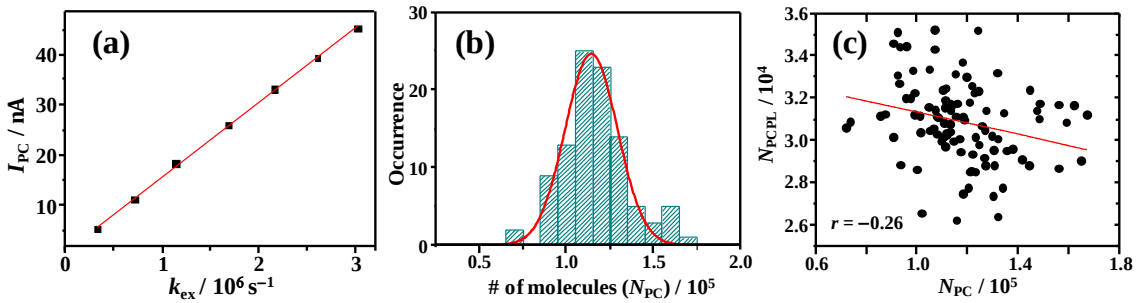

Figure 6. (**a**) Excitation rate dependence of short-circuit PC of the PC-dye. (**b**) Histogram of the number of PC-dye molecules (N_{PC}) at 100 different local positions of a MK-2-DSSC. (**c**) Correlation plot between N_{PCPL} and N_{PC} (correlation coefficient $r = -0.26$).

As summarized in Table 2, the most abundant dye in the DSSC is the PC-dye (75%) with $\langle\Phi_{inj}\rangle \sim 1$; however, 20% of the adsorbed dye corresponds to the PCPL-dye having inferior electron injection yields of $\Phi_{inj} = 0.59–0.65$. This fact suggests the coexistence of two different adsorption modes of MK-2 on the TiO_2 surface. The MK-2 dye possesses a cyanoacrylic acid moiety (=C(−C≡N)COOH) as both electron acceptor and anchoring group (Figure 1c). Previous experimental and theoretical works on the adsorption modes of cyanoacrylic dyes on TiO_2 have shown the coexistence of bidentate and tridentate bridging configurations on TiO_2 [29–31]. According to a recent theoretical study reported by Tsai and coworkers [31], the bidentate configuration is a kinetically trapped adsorption mode, and the tridentate configuration is thermodynamically the most stable. Considering this, it seems reasonable to conclude that the most abundant PC-dye of MK-2 may have a tridentate configuration, whereas the adsorption mode of the PCPL-dye may be bidentate.

4. Conclusions

In summary, the spatially resolved PC and PL analysis of the MK-2-DSSCs reveals three types of dye coexisting in the DSSCs: (i) a dye that only generates PC (PC-dye, 75%), (ii) a dye that generates both PC and PL (PCPL-dye, 20%), and (iii) a dye that only generates PL (PL-dye, 5%). We propose that the PC-dye and the PCPL-dye are chemisorbed on the TiO_2 surface with different adsorption modes (probably tridentate and bidentate bridging configurations, respectively), whereas the PL-dye corresponds to noncovalently trapped molecules within the mesoporous TiO_2 film. Obviously, the photocoversion efficiency of DSSCs can be improved by reducing the number of photoluminescent dyes. We believe that our LSM approach can provide quantitative knowledge on the photoluminescent dyes, which are ubiquitous in DSSCs, and thereby pave the way for decreasing the number of photoluminescent dyes in DSSCs.

Author Contributions: Conceptualization, M.M.; methodology, M.M. and K.M.; validation, M.M. and K.M.; formal analysis, K.M. and R.K.; investigation, K.M. and R.K.; data curation, M.M., K.M., and R.K.; writing—original draft preparation, M.M. All authors have read and agreed to the published version of the manuscript.

Funding: This research was funded by Grants-in-Aid for Scientific Research (C), No. 24550018, Challenging Exploratory Research, No.23655007, and Basic Science Research Projects from The Sumitomo Foundation, No.130550.

Acknowledgments: This work is supported by Grants-in-Aid for Scientific Research (C), No. 24550018, Challenging Exploratory Research, No. 23655007, and Basic Science Research Projects from The Sumitomo Foundation, No. 130550.

Conflicts of Interest: The authors declare no conflict of interest.

References

1. O'Regan, B.; Grätzel, M. A low-cost, high-efficiency solar cell based on dye-sensitized colloidal TiO_2 films. *Nature* **1991**, *353*, 737–740. [CrossRef]

2. Mishra, A.; Fischer, M.K.R.; Bäuerle, P. Metal-free organic dyes for dye-sensitized solar cells: From structure: Property relationships to design rules. *Angew. Chem. Int. Ed.* **2009**, *48*, 2474–2499. [CrossRef] [PubMed]
3. Hagfeldt, A.; Boschloo, G.; Sun, L.; Kloo, L.; Pettersson, H. Dye-sensitized solar cells. *Chem. Rev.* **2010**, *110*, 6595–6663. [CrossRef] [PubMed]
4. Urbani, M.; Grätzel, M.; Nazeeruddin, M.K.; Torres, T. Meso-substituted porphyrins for dye-sensitized solar cells. *Chem. Rev.* **2014**, *114*, 12330–12396. [CrossRef]
5. Bell, T.D.M.; Pagba, C.; Myahkostupov, M.; Hofkens, J.; Piotrowiak, P. Inhomogeneity of electron injection rates in dye-sensitized TiO_2: Comparison of the mesoporous film and single nanoparticle behavior. *J. Phys. Chem. B* **2006**, *110*, 25314–25321. [CrossRef]
6. Ziółek, M.; Martín, C.; Sun, L.; Douhal, A. Effect of electrolyte composition on electron injection and dye regeneration dynamics in complete organic dye sensitized solar cells probed by time-resolved laser spectroscopy. *J. Phys. Chem. C* **2012**, *116*, 26227–26238. [CrossRef]
7. Kilsa, K.; Mayo, E.I.; Kuciauskas, D.; Villahermosa, R.; Lewis, N.S.; Winker, J.R.; Gray, H.B. Effects of bridging ligands on the current-potential behavior and interfacial kinetics of ruthenium-sensitized nanocrystalline TiO_2 photoelectrodes. *J. Phys. Chem. A* **2003**, *107*, 3379–3383. [CrossRef]
8. Bräm, O.; Cannizzo, A.; Chergui, M. Ultrafast fluorescence studies of dye sensitized solar cells. *Phys. Chem. Chem. Phys.* **2012**, *14*, 7934–7937. [CrossRef]
9. Wang, L.; Wang, H.Y.; Fang, H.H.; Wang, H.; Yang, Z.Y.; Gao, B.R.; Chen, Q.D.; Han, W.; Sun, H.B. Universal electron injection dynamics at nanointerfaces in dye-sensitized solar cells. *Adv. Funct. Mater.* **2012**, *22*, 2783–2791. [CrossRef]
10. Rehm, J.M.; McLendon, G.L.; Nagasawa, Y.; Yoshihara, K.; Moser, J.; Gratzel, M. Femtosecond electron-transfer dynamics at a sensitizing dye-semiconductor (TiO_2) interface. *J. Phys. Chem.* **1996**, *100*, 9577–9578. [CrossRef]
11. Burfeindt, B.; Hannappel, T.; Storck, W.; Willig, F. Measurement of temperature-independent femtosecond interfacial electron transfer from an anchored molecular electron donor to a semiconductor as acceptor. *J. Phys. Chem.* **1996**, *100*, 16463–16465. [CrossRef]
12. Martini, I.; Hodak, J.H.; Hartland, G.V. Dynamics of semiconductor-to-dye electron transfer for anthracene dyes bound to different sized TiO_2 particles. *J. Phys. Chem. B* **1999**, *103*, 9104–9111. [CrossRef]
13. Benko, G.; Kallioinen, J.; Korppi-Tommola, J.E.I.; Yartsev, A.P.; Sundstrom, V. Photoinduced ultrafast dye-to-semiconductor electron injection from nonthermalized and thermalized donor states. *J. Am. Chem. Soc.* **2002**, *124*, 489–493. [CrossRef] [PubMed]
14. Piotrowiak, P.; Galoppini, E.; Wei, Q.; Meyer, G.J.; Wiewior, P. Subpicosecond photoinduced charge injection from "molecular tripods" into mesoporous TiO_2 over the distance of 24 angstroms. *J. Am. Chem. Soc.* **2003**, *125*, 5278–5279. [CrossRef] [PubMed]
15. Scott, M.J.; Woodhouse, M.; Parkinson, B.A.; Elliott, C.M. Spatially resolved current-voltage measurements—evidence for nonuniform photocurrents in dye-sensitized solar cells. *J. Electrochem. Soc.* **2008**, *155*, B290–B293. [CrossRef]
16. Navas, J.; Alcántara, R.; Fernández-Lorenzo, C.; Martín-Calleja, J. *Solar Cells-Silicon Wafer-Based Technologies*; Kosyachenko, L.A., Ed.; InTech: London, UK, 2011; ISBN 978-953-307-747-5.
17. Macht, B.; Turrión, M.; Barkschat, A.; Salvador, P.; Ellmer, K.; Tributsch, H. Patterns of efficiency and degradation in dye sensitization solar cells measured with imaging techniques. *Sol. Energy Mater. Sol. Cells* **2002**, *73*, 163–173. [CrossRef]
18. Guillén, E.; Casanueva, F.; Anta, J.A.; Vega-Poot, A.; Oskam, G.; Alcántara, R.; Fernández-Lorenzo, C.; Martín-Calleja, J. Photovoltaic performance of nanostructured zinc oxide sensitized with xanthene dyes. *J. Photochem. Photobiol. A* **2008**, *200*, 364–370. [CrossRef]
19. Navas, J.; Alcántara, R.; Fernandez-Lorenzo, C.; Martín-Calleja, J. A Methodology for improving laser beam induced current images of dye sensitized solar cells. *Rev. Sci. Instrum.* **2009**, *80*, 063102–1–063102-7. [CrossRef]
20. Mitsui, M.; Kawano, Y.; Mori, K.; Wakabayashi, N. Correlations between photovoltaic characteristics, adsorption number, and regeneration kinetics in dye-sensitized solar cells revealed scanning photocurrent microscopy. *Langmuir* **2015**, *31*, 7158–7165. [CrossRef]
21. Wang, Z.S.; Koumura, N.; Cui, Y.; Takahashi, M.; Sekiguchi, H.; Mori, A.; Kubo, T.; Furube, A.; Hara, K. Hexylthiophene-functionalized carbazole dyes for efficient molecular photovoltaics: Tuning of solar-cell performance by structural modification. *Chem. Mater.* **2008**, *20*, 3993–4003. [CrossRef]

22. Zhang, X.H.; Ogawa, J.; Sunahara, K.; Cui, Y.; Uemura, Y.; Miyasaka, T.; Furube, A.; Koumura, N.; Hara, K.; Mori, S. Alternation of charge injection and recombination in dye-sensitized solar cells by the addition of nonconjugated bridge to organic dyes. *J. Phys. Chem. C* **2013**, *117*, 2024–2031. [CrossRef]
23. Koumura, N.; Wang, Z.S.; Mori, S.; Miyashita, M.; Suzuki, E.; Hara, K. Alkyl-functionalized organic dyes for efficient molecular photovoltaics. *J. Am. Chem. Soc.* **2006**, *128*, 14256–14257. [CrossRef] [PubMed]
24. Mitsui, M.; Kawano, Y.; Takahashi, R.; Fukui, H. Photophysics and photostability of 9,10-bis(phenylethynyl)anthracene revealed by single-molecule spectroscopy. *RSC Adv.* **2012**, *2*, 9921–9931. [CrossRef]
25. Park, S.H.; Roy, A.; Beaupré, S.; Cho, S.; Coates, N.; Moon, J.S.; Moses, D.; Leclerc, M.; Lee, K.; Heeger, A.J. Bulk heterojunction solar cells with internal quantum efficiency approaching 100%. *Nat. Photonics* **2009**, *3*, 297–302. [CrossRef]
26. Sun, Z.; Liang, M.; Chen, J. Kinetics of iodine-free redox shuttles in dye-sensitized solar cells: Interfacial recombination and dye regeneration. *J. Acc. Chem. Res.* **2015**, *48*, 1541–1550. [CrossRef]
27. Valeur, B. *Molecular Fluorescence: Principles and Applications*; Wiley-VCH: Weinheim, Germany, 2001.
28. Daeneke, T.; Mozer, A.J.; Uemura, Y.; Makuta, S.; Fekete, M.; Tachibana, Y.; Koumura, N.; Bach, U.; Spiccia, L. Dye regeneration kinetics in dye-sensitized solar cells. *J. Am. Chem. Soc.* **2012**, *134*, 16925–16928. [CrossRef]
29. Jiao, Y.; Zhang, F.; Grätzel, M.; Meng, S. Structure-property relations in all-organic dye-sensitized solar cells. *Adv. Funct. Mater.* **2013**, *23*, 424–429. [CrossRef]
30. Zhang, F.; Ma, W.; Jiao, Y.; Wang, J.; Shan, X.; Li, H.; Lu, X.; Meng, S. Precise identification and manipulation of adsorption geometry of donor-π-acceptor dye on nanocrystalline TiO_2 films for improved photovoltaics. *ACS Appl. Mater. Interfaces* **2014**, *6*, 22359–22369. [CrossRef]
31. Tsai, H.G.; Hu, J.; Tan, C.; Sheng, Y.; Chiu, C. First-principle characterization of the adsorption configurations of cyanoacrylic dyes on TiO_2 film for dye-sensitized solar cells. *J. Phys. Chem. A* **2016**, *120*, 8813–8822. [CrossRef]